Oxalate coprecipitation route to the piezoelectric $Pb(Zr,Ti)O_3$ oxide

Jin-Ho Choy,* Yang-Su Han and Seung-Joo Kim

Department of Chemistry, Center for Molecular Catalysis, Seoul National University, Seoul 151-742, Korea

A homogeneous and stoichiometric $Pb(Zr,Ti)O_3$ (PZT) fine powder was prepared by thermal decomposition of the metal oxalate precursor formed by the precipitation reaction of the metallic components in aqueous solution with oxalic acid. Theoretical solubility isotherms of metal oxalates were established as a function of the solution pH and the metal ion concentration using thermodynamic equilibrium constants for the corresponding metal salts in aqueous solution. Through the theoretical solubility isotherms, the optimum pH domain for preparing the homogeneous and stoichiometric PZT–oxalate precursor was found to be 3–4. Crystalline PZT with tetragonal symmetry began to form after heating the precursor at 600 °C and a monophasic PZT powder consisting of submicrometer (0.3–0.5 μm) particles with spherical shape could be obtained after calcination at 800 °C for 2 h. The oxalate-derived PZT powder showed a good sinterability even below 1150 °C where the piezoelectric properties were optimized.

Lead zirconate titanates, $Pb(Zr_xTi_{1-x})O_3$ (PZT), are of interest owing to their ferroelectric, piezoelectric and other electrical properties.[1,2] The electromechanical response of these materials reaches a maximum near $x \approx 0.52$, which corresponds to the composition of morphotropic phase boundary (MPB) between Ti-rich tetragonal (T) and Zr-rich rhombohedral (R) phases.

Conventionally PZT powders are prepared by solid-state reaction using the constituent oxides PbO, ZrO_2 and TiO_2.[3–6] However, the uniform distribution of Zr/Ti ions at the B-site of the ABO_3 perovskite structure cannot be ensured because the conversion into PZT involves long-range diffusion leading to frozen-in compositional fluctuation. Furthermore, completion of the reaction by long-range diffusion also requires higher temperature (> 1000 °C) and long reaction periods.

Alternatively, chemical routes to PZT *via* suitable precursors have attracted wide attention, these include the hydrolysis of metal alkoxides,[7–9] the freeze- and spray-drying of mixed salt solutions,[10,11] the liquid mix technique (or Pechini process),[12] and the coprecipitation of metal hydroxides[13–15] and oxalates.[16–17] The main advantage of such processes lies in the lowering of reaction temperature, since the atomic or molecular level mixing of constituent metal ions is possible in solution, which also allows the preparation of fine and homogeneous oxide powders with better reactivity and sinterability.

Among wet chemical routes, coprecipitation is known to be quite simple and convenient in achieving high quality oxide powders,[16–22] even though some problems mainly related to cation non-stoichiometry and homogeneity are still unresolved. Generally, coprecipitation is carried out by preparing aqueous solutions of the constituent metals (in the form of nitrates, acetates and chlorides) and of a titrant such as hydroxide and oxalate; the metallic solutions and titrant ones are then mixed together, coprecipitated, filtered, washed and finally calcined. A desired stoichiometry and homogeneity, however, may be lost during coprecipitation when there is a large difference in solubility between the precipitates. In particular, it is very difficult to find an optimum coprecipitation condition in multicomponent systems. In addition, the experimental conditions for preparing powders with a particular stoichiometry have, so far, been determined empirically, and few studies have attempted to examine on a theoretical basis, for example, the effect of solution pH, metal ion concentration, the presence of competing anions, *etc.* In previous reports,[23–28] we made an attempt to establish simple thermodynamic solubility models based on stability and solubility diagrams to predict the optimum processing conditions for preparing functional oxide particles by wet chemical methods. It was found that such a theoretical model could be successfully applied to the preparation of fine homogeneous and stoichiometric powders with high purity and good sinterability.

In the present study, our primary attention was aimed towards the preparation of homogeneous and stoichiometric PZT powders by oxalate coprecipitation. First, a theoretical solubility model has been proposed to predict the optimum precipitation conditions. Secondly, an attempt was made to verify the reliability of our model calculation experimentally by preparing and analyzing the coprecipitated PZT samples. Finally, the powder characteristics, sinterability and piezoelectric properties of the oxalate-derived PZT has been thoroughly investigated.

Theoretical solution modelling

The characteristics of a powder prepared by a solution route are highly dependent upon the chemical species present in the solution, the nature of chemical species also being influenced by solution variables such as pH, temperature, concentration, and so on.[23–28] From this point of view, solubility isotherms which reveal the stability domains of various chemical species as a function of pH *vs.* metal ion concentration ($\log[M^{z+}]$) may be very helpful in determining optimum processing conditions.

Chemical species involved in coprecipitation

The possible chemical species involved in the coprecipitation process are given in Table 1, and their equilibrium reactions and constants considered in the present study are summarized in Table 2. According to Table 1, numerous complex chemical species might be possible by combination of various solution species. Fortunately, however, certain chemical species can be

Table 1 Possible aqueous species involved in the present study

precursor	aqueous species
$Pb(NO_3)_2$	Pb^{2+}, Zr^{4+}, Ti^{4+}
$ZrOCl_2 \cdot 8H_2O$	Cl^-
$TiCl_4$	NO_3^-
NH_4OH	NH_4^+, OH^-
H_2O_2	H_2O_2
CO_2 (from air)	HCO_3^-, CO_3^{2-}
$H_2C_2O_4$	$HC_2O_4^-$, $C_2O_4^{2-}$

Table 2 Equilibria and their constants used in this calculation

no.	equilibria	symbol	log of constant	ref.
1	$H_2C_2O_4 = H^+ + HC_2O_4^-$	K_1	−1.20	31
2	$HC_2O_4^- = H^+ + C_2O_4^{2-}$	K_2	−3.67	31
3	$PbC_2O_4(s) = Pb^{2+} + C_2O_4^{2-}$	K_{sp}	−8.45	32
4	$PB^{2+} + C_2O_4^{2-} = Pb(C_2O_4)^0(aq)$	β_1	3.70	32
5	$Pb^{2+} + 2C_2O_4^{2-} = Pb(C_2O_4)_2^{2-}$	β_2	5.50	32
6	$4HPO^{2-} + 4H_2O + C_2O_4^{2-} = 3Pb(OH)_2 \cdot PbC_2O_4^0(s) + 6OH^-$	K_{sp}	3.28	33
7	$Pb^{2+} + H_2O = Pb(OH)^+ + H^+$	β_1*	−7.71	34
8	$PB^{2+} + 2H_2O = Pb(OH)_2^0(aq) + 2H^+$	β_2*	−17.01	34
9	$Pb^{2+} + 3H_2O = Pb(OH)_3^- + 3H^+$	β_3*	−28.06	34
10	$Pb(OH)_2(s) = Pb^{2+} + 2OH^-$	K_{sp}	−15.3	35
11	$Zr(OH)_2(C_2O_4)(s) = Zr(OH)^{2+} + C_2O_4^{2-}$	K_{sp}	−10.0	36
12	$Zr(OH)^{2+} + C_2O_4^{2-} = Zr(OH)_2(C_2O_4)^0(aq)$	β_1	−6.68	37
13	$Zr(OH)^{2+} + 2C_2O_4^{2-} = Zr(OH)_2(C_2O_4)_2^{2-}$	β_2	−3.34	37
14	$Zr^{4+} + H_2O = Zr(OH)^{3+} + H^+$	β_1*	0.30	34
15	$Zr^{4+} + 2H_2O = Zr(OH)_2^{2+} + 2H^+$	β_2*	−1.70	34
16	$Zr^{4+} + 3H_2O = Zr(OH)_3^+ + 3H^+$	β_3*	−5.10	34
17	$Zr^{4+} + 4H_2O = Zr(OH)_4^0(aq) + 4H^+$	β_4*	−9.70	34
18	$Zr^{4+} + 5H_2O = Zr(OH)_5^- + 5H^+$	β_5*	−16.00	34
19	$Zr(OH)_4(s) = Zr^{4+} + 4OH^-$	K_{sp}	−52.0	38
20	$Ti(OH)_2^{2+} + C_2O_4^{2-} = Ti(OH)_2(C_2O_4)^0(aq)$	β_1	7.90	37
21	$Ti(OH)_2^{2+} + 2C_2O_4^{2-} = Ti(OH)_2(C_2O_4)_2^{2-}$	β_2	13.20	37
22	$PbTiO(C_2O_4)_2(s) = Pb^{2+} + Ti(OH)_2^{2+} + 2C_2O_4^{2-}$	K_{pto}	−6.90	37
23	$TiO^{2+} + H_2O = TiO(OH)^+ + H^+$	β_1*	−1.60	34
24	$TiO^{2+} + 2H_2O = TiO(OH)_2^0(aq) + 2H^+$	β_2*	−4.10	34
25	$TiO(OH)_2(s) = TiO^{2+} + 2OH^-$	K_{sp}	−27.9	34

β* = overall stability constants representing the protolytic equilibria; β = overall stability constant; k = normal stability constant; K_{sp} = solubility product.

excluded successfully by considering their solubility. For instance, nitrates such as $Pb(NO_3)_3$, $ZrO(NO_3)_2$ and $TiO(NO_3)_2$ exhibit relatively high solubility in aqueous solution. Moreover, in the presence of oxalates, the contribution of these nitrate complex species to the overall solubility becomes negligible. Among possible metal chloride complexes, zirconium and titanium chloride compounds show high solubility in aqueous solution and the formation of soluble species also seems to be unlikely in the presence of organic ligands such as oxalates. While $PbCl_2$ can be formed as a stable solid phase owing to its low solubility in acidic aqueous solution,[28] its formation is strongly suppressed in the presence of oxalic acid owing to the strong chelating ability of the lead ion, which has no practical influence on the overall solubility of the lead system. Ammonium ions which originate from NH_3(aq) may also react with counter anions to form various ammonium salts such as NH_4Cl, $(NH_4)_2C_2O_4$ and NH_4NO_3, which are highly soluble in aqueous solution. Metal-containing ammonium salts such as $(NH_4)_2TiO(C_2O_4)_2$ and $(NH_4)_2ZrO(C_2O_4)_2$ are also highly soluble in aqueous solution, so they are unlikely to form stable precipitates even though soluble species may contribute to the solubility of oxalates to some extent.

The presence of H_2O_2 alters the solution chemistry of metal species owing to its high oxidation potential. When H_2O_2 is added to an aqueous solution containing Ti^{4+}, various types of peroxotitanium(IV) species may be formed. Although there has been much confusion over the exact peroxotitanium species, it is generally accepted that $Ti(OH)_2(H_2O_2)^{2+}$ (or TiO^{2+}) is present as the dominant species in acidic solution.[28] In the presence of H_2O_2, Pb^{2+} is oxidized to Pb_3O_4 in basic solution and the formation of a lead carbonate precipitate is strongly suppressed. For Zr^{4+}, the complexation of zirconium by hydrogen peroxide in aqueous solution results in formation of the peroxozirconium complex $Zr_4(O_2)_2(OH)_4^{8+}$. The effect of H_2O_2 in the solution chemistry of lead and zirconium, however, was not included here because we used H_2O_2 only for the preparation of peroxotitanium solution separately by mixing $TiCl_4$ and H_2O_2-containing distilled water.

All the metal cations show extensive hydrolysis in aqueous solution to form various hydrolyzed complexes of monomeric and polymeric forms depending upon the solution pH and metal ion concentrations. In some cases, polynuclear species exert a significant effect on the solubility and exist as dominant soluble species, especially at acidic pH. In our previous report,[28] the effect of polymeric species like $Pb_6(OH)_8^{4+}$, $Zr_4(OH)_8^{4+}$ and $(TiO)_8(OH)_{12}^{4+}$ on the solubility of hydroxide precipitation was discussed in detail.

Concerning the oxalate complexes, the chemical species and their equilibrium constants in the lead(II)–oxalate system are well defined. In the present study, PbC_2O_4(s) and $3Pb(OH)_2 \cdot PbC_2O_4$(s) are regarded as the possible solid species and $Pb(C_2O_4)^0$(aq) and $Pb(C_2O_4)_2^{2-}$ as the dominant soluble species. On the other hand, the hydrolytic behavior and complex equilibria of zirconium(IV)– and titanium(IV)–oxalic acid systems have proved to be exceedingly complicated.[39] It has been reported that $Zr(C_2O_4)_2$(s) and $Zr(OH)_2(C_2O_4)$(s) are the possible precipitation phases in the zirconium(IV)–oxalic acid system even though there is some uncertainty in chemical formulae and equilibrium constants. As soluble species, $Zr(OH)_2(C_2O_4)^0$(aq) and $Zr(OH)_2(C_2O_4)_2^{2-}$ are included in predicting the solubility behavior of the zirconium–oxalate system. Even though the formation of pure titanium oxalate, $TiO(C_2O_4)$(s) or $Ti(OH)_2(C_2O_4)$(s), in aqueous solution is still controversial, the coprecipitation with divalent cations to form $ATiO(C_2O_4)_2 \cdot xH_2O$(s) (A = Ba^{2+}, Sr^{2+}, Pb^{2+}, *etc.*) has been well defined. Thus, in this work, lead titanyloxalate, $PbTiO(C_2O_4)_2$(s), is considered as a stable solid phase, while $Ti(OH)_2(C_2O_4)^0$(aq) and $Ti(OH)_2(C_2O_4)_2^{2-}$ are soluble species.

Based on the above discussion, we can sum up the possible chemical species which have significant influence on the solubility of the lead(II)–zirconium(IV)–titanium(IV)–oxalic acid–water system. In the presence of oxalic acid, most metal salts except for hydroxides can be excluded owing to the strong chelating ability of oxalic acid to metal hydroxides, and oxalate salts are listed in Table 2. Since the basic principle underlying the methodology in constructing the solubility isotherms can be found in the literature,[29,30] details of numerical calculations are not included here. Since the metal ions are equilibrated

with ligands, the distribution of chemical species in an aqueous solution is generally expressed as a function of ligand (oxalate) concentration. However, it is more practical to express it as a function of pH because the hydroxide anion always exists as a competing ligand in aqueous solution. Therefore, we have regarded the pH instead of $[C_2O_4^{2-}]$ as a master variable to control the equilibrium reaction in the present study.

Dissociation of oxalic acid

Oxalic acid, $H_2C_2O_4$, is a weak diprotic acid, it dissociates in a stepwise manner in solution depending upon pH, and the following chemical equilibria are well defined;

$$H_2C_2O_4 = H^+ + HC_2O_4^- \qquad \log K_1 = -1.20$$

$$HC_2O_4^- = H^+ + C_2O_4^{2-} \qquad \log K_2 = -3.67$$

From the mass law and charge neutrality principle of the oxalic acid system, the concentrations of oxalate species can be expressed as follows;

$$[C_2O_4^{2-}] = \alpha_{C_2O_4} A_T = [(K_1K_2)/([H^+]^2 + K_1[H^+] + K_1K_2)]A_T \quad (1)$$

where $\alpha_{C_2O_4}$ is the ionization fraction of oxalate anion, $[C_2O_4^{2-}]$, and A_T is the total concentration of oxalates ($A_T = [H_2C_2O_4] + [HC_2O_4] + [C_2O_4^{2-}]$) in mol dm^{-3}. Introducing the equilibrium constants (K_1 and K_2) and total concentration (1.0 mol dm^{-3}), the concentrations of oxalate species ($\log C_i$) are given as a function of pH. According to the resulting $\log C_i$–pH diagram (Fig. 1), three oxalate species $H_2C_2O_4$, $HC_2O_4^-$ and $C_2O_4^{2-}$ exist as major species in the pH ranges <1.20, 1.20–3.67 and >3.67, respectively.

Solubility of the lead(II)–oxalic acid–water system

The numerical details used in constructing the solubility diagrams of metal oxalates are given here for the lead(II)–oxalic acid–water system as a model case. According to the literature,[32] the solubility equilibrium for lead oxalate is given by;

$$Pb(C_2O_4)(s) = Pb^{2+} + C_2O_4^{2-} \qquad \log K_{sp} = -8.45 \quad (2)$$

Rearranging and taking logarithms gives

$$\log[Pb^{2+}] = \log K_{sp} - \log[C_2O_4^{2-}] \quad (3)$$

Introducing the K_{sp} value and eqn. (1) into eqn. (3), gives the Pb^{2+} concentration which is equilibrated with solid $Pb(C_2O_4)(s)$ as a function of pH as shown in Fig. 2.

Besides the solubility equilibrium, Pb^{2+} can complex with oxalate and hydroxide anions forming various soluble species

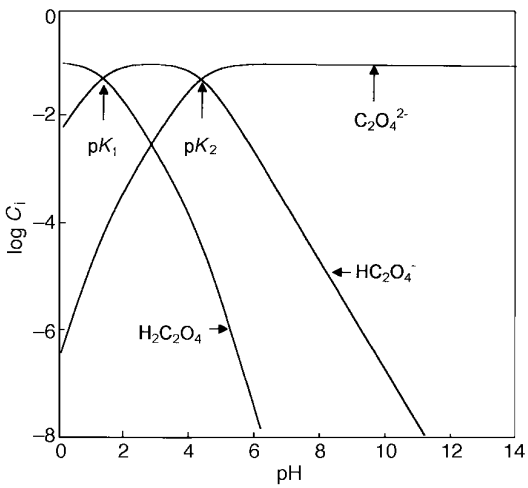

Fig. 1 Log C_i–pH diagram for the diprotic oxalic acid at 25 °C

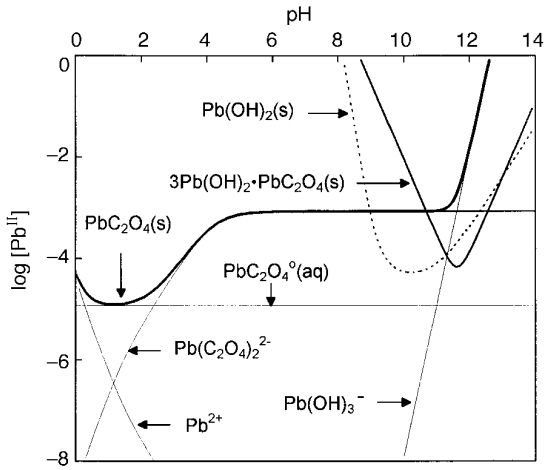

Fig. 2 Solubility diagram of the Pb^{II}–oxalic acid–H_2O system at 25 °C

such as $Pb(C_2O_4)^0(aq)$, $Pb(C_2O_4)_2^{2-}$, $Pb(OH)_2{}^0(aq)$, *etc.* For example, the equilibrium reaction of $Pb(C_2O_4)^0(aq)$ is given as follows;

$$Pb^{2+} + C_2O_4^{2-} = Pb(C_2O_4)^0(aq) \quad \log \beta_1 = -3.70 \quad (4)$$

Also, rearranging and taking logarithms, eqn. (4) can be rearranged to eqn. (5)

$$\log[Pb(C_2O_4)^0(aq)] = \log[Pb^{2+}] + \log \beta_1 + \log[C_2O_4^{2-}] \quad (5)$$

Introducing the β_1 value and substituting $\log[Pb^{2+}]$ into eqn. (3), enables the $Pb(C_2O_4)^0(aq)$ concentration equilibrated with solid $PbC_2O_4(s)$ to be plotted *vs.* pH.

A basic lead oxalate salt of formula $3Pb(OH)_2{\cdot}PbC_2O_4(s)$ was also reported[33] in the lead(II)–oxalic acid–water system with the following equilibrium reaction;

$$4HPbO_2^- + 4H_2O + C_2O_4^{2-} = 3Pb(OH)_2{\cdot}PbC_2O_4(s) + 4OH^- \quad \log \beta_{sp} = -3.70 \quad (6)$$

The solubility curve for the above equilibrium was also compared with those of lead hydroxide and oxalate precipitates in Fig. 2. The thick solid and dotted lines denote the total concentrations of soluble species saturated with corresponding solid lead oxalates [$PbC_2O_4(s)$ and $3Pb(OH)_2{\cdot}PbC_2O_4(s)$] and hydroxide [$Pb(OH)_2(s)$], respectively.

The solubility minimum (maximum precipitation) of lead oxalate occurs at a pH of *ca.* 1.0. In this pH range, a stoichiometric precipitation of $PbC_2O_4(s)$ is expected with a yield of $>99.99\%$ when initial $[Pb^{2+}] = 0.1$ mol dm^{-3}. As the solution pH is increased (pH > 2.4), the oxalate precipitate may partly dissolve by the ligation of oxalate to form a $Pb(C_2O_4)_2^{2-}$ species. The simple overlap of solubility curves of lead hydroxide and oxalates indicates that the pure lead hydroxide is unlikely to form in the presence of oxalate even under quite basic pH conditions. As the solution pH increases, however, it is evident that more hydroxide anions may take part in the complexation, leading to the formation of mixed-ligand lead salts. The overlap of solubility curves of $PbC_2O_4(s)$ and $3Pb(OH)_2{\cdot}PbC_2O_4(s)$ shows that the basic lead salt becomes more stable than the pure oxalate above pH = 10.7, and the basic lead salt reaches a minimum solubility at pH *ca.* 11.7. The precipitation of the basic lead salt, $3Pb(OH)_2{\cdot}PbC_2O_4(s)$, was reported experimentally at pH *ca.* 12,[33] which is in good agreement with our theoretical expectation.

Solubility of the zirconium(IV)–oxalic acid–water system

The solubility curves obtained by applying the same methodology used for lead oxalate are plotted as a function of pH

(Fig. 3). For comparison, the solubility curve of $Zr(OH)_4(s)$ which is in equilibrium with soluble hydroxy and oxalate species are also superimposed in this figure. The precipitation region of $Zr(OH)_2(C_2O_4)(s)$ is confined to $pH < 3.5$ owing to its relatively large solubility and strong hydrolysis tendency of Zr^{4+}. Since Zr^{4+} has a higher charge-to-size ratio than Pb^{2+}, the effect of hydrolysis on the solubility is thought to be more significant. Thus, beyond $pH = 3.5$, $Zr(OH)_4(s)$ becomes more stable than $Zr(OH)_2(C_2O_4)(s)$. As for the Pb system, a basic zirconium oxalate such as $Zr(C_2O_4)_2 \cdot xZr(OH)_4(s)$ would be expected in the pH range of 3–9.

Solubility of the titanium(IV)–oxalic acid–water–hydrogen peroxide system

The expected compounds in the titanium(IV)–oxalic acid–H_2O–H_2O_2 system are titanium oxalates, hydroxides and peroxotitanium species. Because the precipitation of pure titanium oxalate, $TiO(C_2O_4)(s)$ or $Ti(OH)_2(C_2O_4)$, in aqueous solution is still not well characterized and its solubility constant has not been determined yet, we have considered $TiO(OH)_2(s)$ as a possible solid phase. The effects of polymeric species such as $(TiO)_8(OH)_{12}^{4+}$ and hydrogen peroxide on the solubility of $TiO(OH)_2(s)$ are discussed in detail in our previous report.[28] It was found that the presence of polymeric species and hydrogen peroxide increased the solubility of titanium hydroxide at acid pH. The addition of oxalate ions to the Ti^{IV}–H_2O–H_2O_2 system also leads to a drastic increase of the solubility of $TiO(OH)_2(s)$ owing to the formation of soluble $Ti(OH)_2(C_2O_4)_2^{2-}$ species. The precipitation of $TiO(OH)_2(s)$ in the Ti^{IV}–oxalic acid–H_2O–H_2O_2 system occurs beyond $pH = 5.7$ when $[Ti^{4+}] = 0.1$ mol dm^{-3}, which is consistent with experiment.[41]

As discussed above, titanium oxalate can be precipitated in the presence of Pb^{2+} to form $PbTiO(C_2O_4)_2(s)$. The solubility isotherm calculated for $PbTiO(C_2O_4)_2(s)$ is shown in Fig. 4. In calculating the solubility isotherm of $PbTiO(C_2O_4)_2(s)$, $[Pb^{2+}]$ was fixed to 0.1 mol dm^{-3} and the isotherm curves of minor species were omitted for simplicity. As to the coprecipitation of titanium oxalate with lead, the formation of $PbTiO(C_2O_4)_2(s)$ begins at pH *ca.* 2 and reaches a maximum at pH *ca.* 5 where stoichiometric precipitation with >99.99% yield would be expected from a 0.1 mol dm^{-3} solution.

Solubility of the lead(II)–zirconium(IV)–titanium(IV)–oxalic acid–water system

To compare the solubility behavior of individual metal oxalates and to predict the optimal coprecipitation conditions, the solubility curves considered so far are superimposed in Fig. 5.

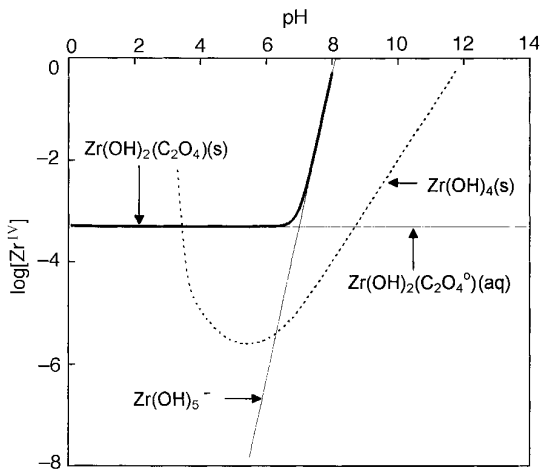

Fig. 3 Solubility diagram of the Zr^{IV}–oxalic acid–H_2O system at 25 °C

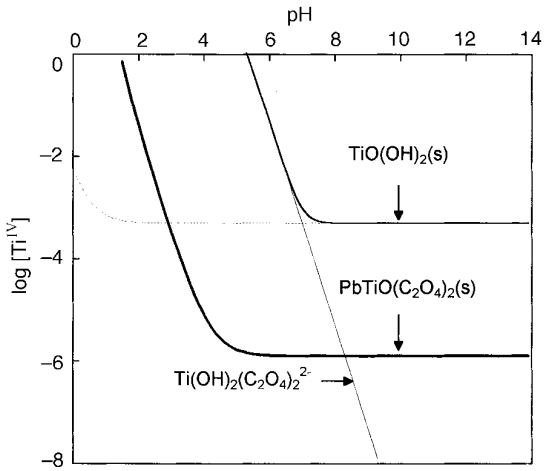

Fig. 4 Solubility diagram of the Pb^{II}/Ti^{IV}–oxalic acid–H_2O system at 25 °C

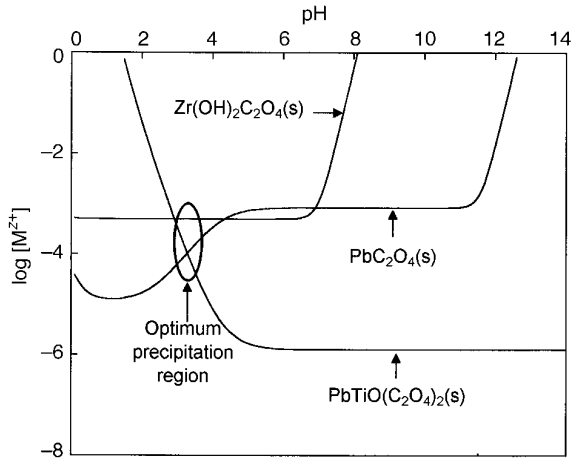

Fig. 5 Solubility diagram of the Pb^{II}–Zr^{IV}–Ti^{IV}–oxalic acid–H_2O system at 25 °C

It is apparent that the simultaneous precipitation region (triple point of solubility curves) of individual oxalates cannot be found in the ternary Pb–Zr–Ti system, which might be responsible for the non-stoichiometry of the oxalate coprecipitates. At $pH < 2$, Pb^{II} and Zr^{IV} ions can be quantitatively precipitated as oxalates, but Ti^{IV} ions remain as soluble species, *e.g.* $Ti(OH)_2(C_2O_4)_2^{2-}$. In the basic pH range, Pb^{II} and Ti^{IV} can be precipitated in the forms of $PbTiO(C_2O_4)_2(s)$ and $PbC_2O_4(s)$ quantitatively, while $Zr(OH)_2C_2O_4(s)$ dissolves owing to the formation of the soluble $Zr(OH)_2(C_2O_4)_2^{2-}$ species. Between pH 4 and 7, stoichiometric precipitates are guaranteed but the formation of pure and homogeneous PZT oxalate precipitates is quite difficult owing to the formation of zirconium hydroxide (Fig. 3) and to large solubility differences. Consequently, to minimize the formation of metal hydroxides and to enhance homogeneous mixing of the constituent metal ions, the optimum pH for quantitative precipitation of the PZT–oxalate precursor can be predicted as *ca.* 3–4 on the basis of solubility diagrams. If we use 0.1 mol dm^{-3} metal ion source solutions, it is expected that >99% of metal oxalate will be precipitated in this pH range.

Experimental

Powder preparation

The starting reagents used were high-purity $Pb(NO_3)_2$ (Aldrich, 99.5%), $TiCl_4$ (Aldrich, 99.9%) and $ZrOCl_2 \cdot 8H_2O$

(Merck, 99%). In preparing the source solution of titanium, titanium tetrachloride (5 ml) was mixed in aqueous H_2O_2 [30% H_2O_2 solution (5 ml) and distilled water (25 ml)], at room temperature to give a *ca.* 1.0 mol dm^{-3} titanium solution, which was filtered in order to remove any titanium hydroxide. Then the precise titanium content of the filtered solution was determined volumetrically by EDTA back titration with a 0.1 mol dm^{-3} lead nitrate standard solution, and finally diluted to give a 0.1 mol dm^{-3} aqueous solution. $Pb(NO_3)_2$ and $ZrOCl_2 \cdot 8H_2O$ were also dissolved in distilled water individually and also diluted to 0.1 mol dm^{-3}. Desired quantities of lead, zirconium and titanium solutions corresponding to the composition of $Pb(Zr_{0.52}Ti_{0.48})O_3$ were titrated simultaneously into a 0.1 mol dm^{-3} oxalic acid solution with a titration rate of *ca.* 5 ml min^{-1} for Ti and Zr solutions and 10 ml min^{-1} for Pb, respectively. During the titration, the solution pH was adjusted to 3.5 ± 0.5, by addition of NH_3(aq) (pH = 12), and the solution was also stirred vigorously to minimize concentration gradients. After titration was complete, the reaction system was allowed to stand for more than 1 h to try and ensure equilibrium. The white precipitate was then filtered off and washed several times with deionized water to remove residual Cl^- and NO_3^- ions. The washed product was dried at 100 °C for 5 h, and heat treated at various temperatures for 2 h under an ambient atmosphere.

Powder characterization

The thermal behavior of the PZT–oxalate precursor was examined with a Rigaku thermal analyzer (TAS-100) from room temperature to 800 °C (heating rate = 10 °C min^{-1}) under ambient atmosphere. The evolution of crystal structure upon calcination at different temperatures was also investigated by powder X-ray diffraction (Philips PW-1830) using Ni-filtered Cu-Kα radiation ($\lambda = 1.5418$ Å). Average particle size and the morphology of the calcined and sintered PZT samples were examined by scanning electron microscopy (SEM) (JSM-8404). The specific surface area was determined by a conventional three-point BET technique at liquid-nitrogen temperature with Quantasorb. Inductively coupled plasma (ICP) (Shimazu ICPS-5000) analyses were also employed for determining the cation stoichiometry of calcined powders and residual solutions after coprecipitation at pH = 3.5.

Sinterability and piezoelectric property measurements

The oxalate-derived PZT powder calcined at 800 °C for 2 h was die-pressed into discs of *ca.* 12 mm in diameter and 1.2 mm thickness under a pressure of 100 kg cm^{-2}. The discs were then sintered at different temperatures from 1050 to 1200 °C for 2 h. The apparent density for sintered samples was measured geometrically, and microstructure was observed by SEM on freshly fractured surfaces.

For measuring piezoelectric properties, the sintered specimens were polished and electroded by brushing with silver paste and subsequently firing at 600 °C for 1 h. Discs were then poled by applying a dc electric field of 3.5 kV mm^{-1} at 100 °C in a silicon oil bath for 30 min. After poling, the specimens were aged for 24 h prior to dielectric and piezoelectric measurements. The piezoelectric properties were determined by a resonance method following IRE standards[42] at 1 kHz. The piezoelectric coefficient d_{33} of the samples was measured using a Berlincourt Piezo-d_{33} meter.

Results and Discussion

Verification of solubility models

The solubility models calculated in the present study are based on the thermodynamic constants. However, some possible species are excluded owing to the lack of solubility data, so the simple solubility isotherms cannot fully describe the dynamic coprecipitation process. Despite this limitation in quantitative analysis, it is still instructive to examine the solubility relations as a qualitative tool for describing the coprecipitation. If the oxalate precursors were precipitated from an acid solution by decreasing pH, a homogeneous precipitate may not be formed owing to large differences in solubility at low pH (Fig. 5), giving rise to the separate formation of each metal oxalate. Conversely, if the metal solution is added slowly to a basic oxalate solution, $PbTiO(C_2O_4)_2$(s) would be rapidly precipitated from the solution, while Zr^{IV} ions remain in solution until a pH of 11 when $Zr(OH)_4$(s) is formed, also leading to an inhomogeneous product. The highest level of supersaturation for each element occurs at pH 3–4, resulting in homogeneous coprecipitated powders.

Table 3 Elemental analysis data for the residual solution after coprecipitation

element	Pb	Zr	Ti
m/m(%)	<0.001	0.088	0.040

Error limit of ICP: <0.001% m/m.

In order to confirm quantitative precipitation, elemental analysis (Table 3) on the residual solution after precipitation was performed using the ICP method. In accordance with theoretical expectation, stoichiometric precipitation with >99.9% yield could be achieved, implying the successful quantitative coprecipitation of PZT–oxalate precursors, which also confirms the reliability of our model calculation. The detection of small amounts of Zr^{IV} and Ti^{IV} in the residual solution might be attributed to the formation of soluble ammonium oxalates $(NH_4)_2ZrO(C_2O_4)_2$ and $(NH_4)_2TiO(C_2O_4)_2$, which were excluded in the theoretical calculation owing to lack of solubility data.

Thermal analysis

TG–DSC curves of the oxalate precipitate are shown in Fig. 6. First, dehydration of oxalate precursor takes place in the range 80–200 °C in two steps. The first stage corresponds to the loss of absorbed water and the second to the loss of crystalline water. Secondly, in the range 220–380 °C, the oxalates decompose in two steps. In air, the oxalate decomposition reaction starts with a weak endotherm followed by an exotherm at *ca.* 340–380 °C mainly due to the oxidative decomposition of the oxalate carbon chain.[16] A drastic mass loss at 220–380 °C in the TG curve also suggests decomposition of the oxalates. An additional weak exothermic peak in the DSC curve at 600 °C

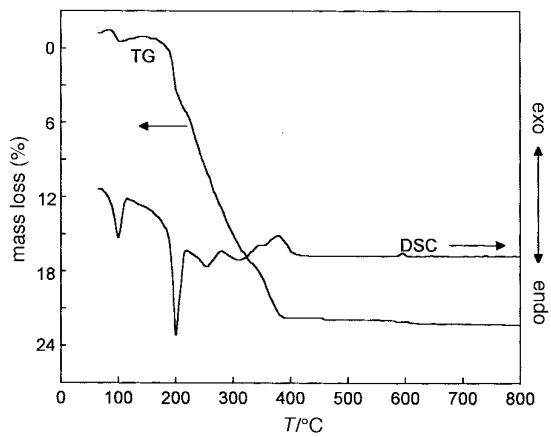

Fig. 6 TG–DSC curves of the PZT–oxalate precursor under ambient atmosphere with a heating rate of 10 °C min^{-1}

without any mass loss in the TG curve can be assigned to the crystallization of the PZT lattice.

Crystallization of PZT

From a series of powder X-ray diffraction patterns of the coprecipitate [Fig. 7(a)] and its calcined products at given temperatures for 2 h [Fig. 7(b)–(d)] it is seen that the freshly precipitated oxalates are essentially amorphous with only a low intensity PbC_2O_4 crystalline phase. The formation of the crystalline PbC_2O_4 phase might be due to the difference in cation stoichiometry in the chemical formula of $Pb(Zr_{0.52}Ti_{0.48})O_3$. According to Fig. 5, some Pb ions would be coprecipitated with Ti ions to form $PbTiO(C_2O_4)_2$ while the remainder preferentially react with oxalate anion, forming the PbC_2O_4 phase rapidly. After calcination at 400 °C, the XRD pattern for the PbC_2O_4 crystalline phase was transformed to a crystalline PbO phase. Upon calcination at 600 °C, the crystalline PZT phase was formed directly without generating $PbTiO_3$ or $PbZrO_3$ as separate phases, and a monophasic PZT was formed after heating at 800 °C. All the reflection patterns could be indexed on the basis of tetragonal symmetry ($a=4.014$, $c=4.119$ Å) corresponding to the composition $Pb(Zr_{0.52}Ti_{0.48})O_3$, and no rhombohedral phase was observed, implying the homogeneous distribution of Ti^{4+} and Zr^{4+} in B-sites of the perovskite lattice.[4,5]

Particle characteristics

Fig. 8 shows a scanning electron micrograph of an oxalate-derived PZT powder calcined at 800 °C for 2 h and the particle characteristics are summarized in Table 4. Well developed spherical shaped particles of size 0.3–0.5 μm are observed. They, however, seem to be formed from agglomeration of small primary particles. This observation was confirmed by comparing particle sizes calculated from X-ray peak broadening effects, BET surface area and SEM observation (Table 4). The X-ray peak broadening indicates a primary particle size of *ca.* 0.044 μm. The specific surface area of 18 $m^2\ g^{-1}$ measured by BET corresponds to the particle size of *ca.* 0.041 μm, those which also give evidence of agglomeration of nanometer sized oxide particles. Elemental analyses for the precipitates and the residual solution indicate that the overall stoichiometry of cations is well retained during the coprecipitation, confirming again that our solubility model is very efficient for obtaining stoichiometric oxide powders.

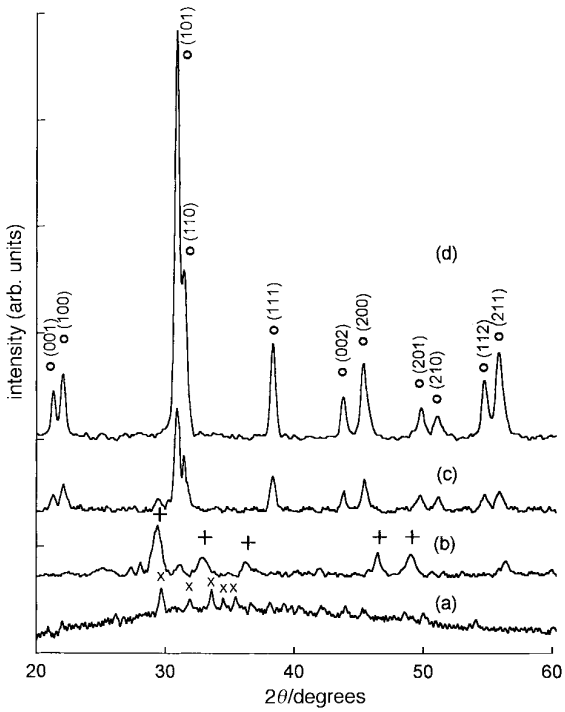

Fig. 7 Powder X-ray diffraction patterns of the coprecipitated and calcined PZT powders at the given temperature for 2 h. (a) Precursor, (b) 400 °C, (c) 600 °C, (d) 800 °C; ○, PZT; ×, PbC_2O_4(s); +, PbO.

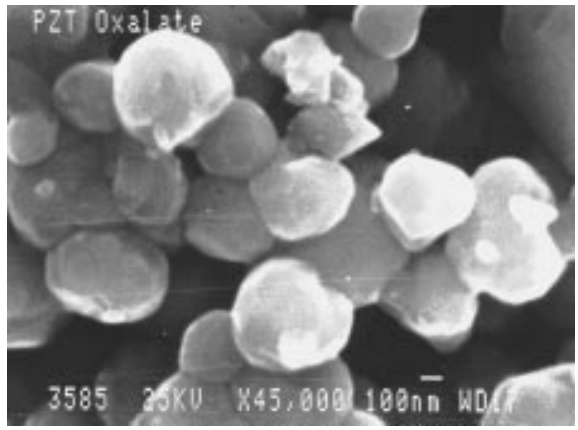

Fig. 8 Scanning electron micrograph of oxalate-derived PZT powder calcined at 800 °C for 2 h

Table 4 Characteristics of the oxalate-derived PZT powder

particle morphology	spherical
particle size/μm (SEM)	0.3–0.5
specific surface area/$m^2\ g^{-1}$ (BET)	18
ESD[a]/μm	0.041
crystallite size[b]/μm	0.044
cation stoichiometry[c]	$Pb_{0.986}(Zr_{0.520}Ti_{0.479})O_3$

[a]ESD = equivalent spherical diameter calculated from surface area; $d=6/S_{BET}\rho$ where S_{BET} = specific surface area ($m^2\ g^{-1}$) and ρ = theoretical density of PZT (8.147 g cm^{-3}). [b]Estimated from X-ray line broadening effect using the Scherrer formula; $t=0.9\lambda/B\cos\theta$ where t = diameter of cystallite, B = broadening of diffraction lines (radians) and λ = wavelength (1.541 84 Å). [c]Determined by inductively coupled plasma (ICP) analysis.

Sintering and piezoelectric properties

In order to study the sinterability and piezoelectric properties of oxalate-derived PZT powders, the relative density of the samples was measured with respect to the sintering temperature, and the piezoelectric parameters were also obtained on the sintered samples with >90% theoretical density, which are summarized in Table 5. A dense PZT sample with a maximum relative density of 96% can be prepared after firing at 1150 °C for 2 h. Conventionally, it is necessary to use a specific buffer atmosphere ($PbO+PbZrO_3$) to achieve completely dense bodies owing to the evaporation of PbO from the pellet surface.[2] Therefore, it can be thought that the present result is quite acceptable taking into account the fact that sintering was carried out using neither a buffer atmosphere

Table 5 Sinterability and piezoelectric properties of PZT samples sintered for 2 h

sintering temperature/°C	1100	1150	1200
relative density(%)	90	96	93
dissipation factor/tanδ	0.034	0.028	0.031
electromechanical coupling coeff./K_p	0.36	0.51	0.38
mechanical quality factor/Q_m	68	92	73
relative permittivity/$\varepsilon_{33}{}^T$ (at 1 kHz)	290	430	390
piezoelectric const./d_{33}	108	155	138

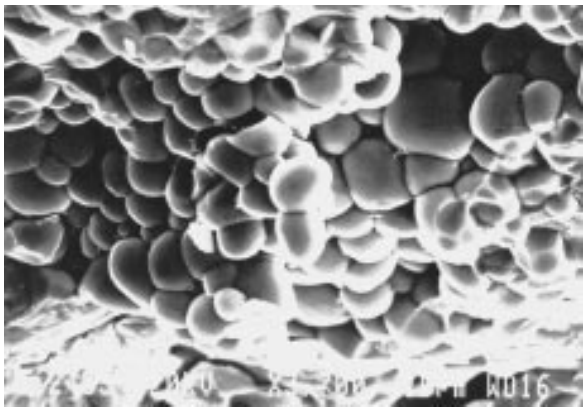

Fig. 9 Scanning electron micrograph on the freshly fractured surfaces of a PZT sample sintered at 1150 °C for 2 h

nor hot-pressing techniques. This enhanced densification at a considerably lower temperature can be attributed to the small particle size and large reactive surface area of oxalate-derived PZT powder which displays good compositional and structural homogeneity. A decrease in the relative density of the sample sintered at 1200 °C might be due to rapid material flow during the sintering originating from the high surface activity of oxalate-derived PZT powders, thereby leading to an entrapment of porosity (closed pores) and subsequent pore coarsening.

According to the scanning electron micrograph on the fractured surfaces of the specimens sintered at 1150 °C for 2 h (Fig. 9), the sintered sample consists of fine and uniform grains of size 2–5 μm, and the shape of grains appears to be nearly spherical with little evidence of faceting.

As listed in Table 5, piezoelectric parameters seem to be closely related to the relative density. The sample sintered at 1150 °C exhibits the best piezoelectric properties. However, despite excellent powder characteristics and sinterability, the piezoelectric properties were not improved significantly. Although the exact cause of this cannot be definitely assigned the isotropic grain shape (Fig. 9) might be responsible for lowering the dielectric and piezoelectric properties.

Conclusions

We propose a simple oxalate route to homogeneous and stoichiometric PZT powders consisting of submicrometer sized particles. On the basis of theoretical consideration of thermodynamic equilibria for metal oxalates in an aqueous solution, the optimum pH condition (3–4) for the coprecipitation of PZT-oxalates could be determined, which was followed by experimental verification. A monophasic PZT powder with good compositional and structural homogeneity was obtained by thermal decomposition of the PZT oxalate precursor at a considerably low temperature of 800 °C. The oxalate-derived PZT powder consisted of submicrometer sized (0.3–0.5 μm) particles and has good sinterability, with 96% of the theoretical density being achieved after firing at 1150 °C for 2 h. This sample exhibited the best piezoelectric properties.

This work was supported in part by the SNU-Daewoo Research Fund (1995) and by the Korean Science and Engineering Foundation (KOSEF) through the Research Center of Excellency 'Center for Molecular Catalysis'.

References

1 B. Jaffe, W. R. Cook and H. Jaffe, *Piezoelectric Ceramics*, Academic Press, New York, 1971.
2 K. Okazaki, *Ferroelectrics*, 1982, **41**, 77.
3 D. L. Hankey and J. V. Biggers, *J. Am. Ceram. Soc.*, 1981, **64**, 172.
4 K. Kakegawa, J. Mohri, S. Shirasaki and K. Takahashi, *J. Am. Ceram. Soc.*, 1982, 65, 515.
5 R. R. Krishnan and P. Ramakrishnan, *Br. Ceram. Trans. J.*, 1988, **87**, 99.
6 T. R. Shrout, P. Papet, S. Kim and G. S. Lee, *J. Am. Ceram. Soc.*, 1990, **73**, 1862.
7 T. Fukui, C. Sakurai and M. Okuyama, *J. Mater. Res.*, 1992, **7**, 791.
8 N. Okada, K. Ishikawa, K. Murakami, T. Nomura, M. Hagino, N. Nishino and U. Kihara, *Jpn. J. Appl. Phys.*, 1992, **31**, 304.
9 C. D. Chandler, C. Roger and M. J. Hampden-Smith, *Chem. Rev.*, 1993, **93**, 1205.
10 R. Lal, R. Krishnan and P. Ramakrishinan, *Mater. Sci. Eng.*, 1987, **96**, L25.
11 R. Lal, N. M. Gokhale, R. Krishnan and P. Ramakrishinan, *J. Mater. Sci.*, 1989, **24**, 2911.
12 M. A. Zaghete, S. O. P. Santos, J. A. Varela, E. Longo and Y. P. Mascarenhas, *J. Am. Ceram. Soc.*, 1992, **75**, 2088.
13 V. R. Palkar and M. S. Multani, *Mater. Res. Bull.*, 1979, **14**, 1353.
14 T. R. N. Kutty and R. Balachandran, *Mater. Res. Bull.*, 1984, **19**, 1479.
15 A. P. Singh, S. K. Mishra, D. Pandey, C. D. Prasad and R. Lal, *J. Mater. Sci.*, 1993, **28**, 5050.
16 R. Balachandran and T. R. N. Kutty, *Mater. Chem. Phys.*, 1984, **10**, 287.
17 H. Yamamura, S. Kuramoto, H. Haneda, A. Watanabe and S. Shirasaki, *J. Ceram. Soc. Jpn.*, 1986, **92**, 470.
18 P. P. Phule and S. H. Risbud, *J. Mater. Sci.*, 1990, **25**, 1169.
19 H. Yamamura, A. Watanabe, S. Shirasaki, Y. Moriyoshi and M. Tanada, *Ceram. Int.*, 1985, **11**, 17.
20 K. Saegusa, W. E. Rhine and H. K. Bowen, *J. Am. Ceram. Soc.*, 1993, **76**, 1495.
21 D. H. Chen, C. Y. Shei, S. R. Sheen and C. T. Chang, *Jpn. J. Appl. Phys.*, 1991, **30**, 1198.
22 M. Dasgupta and S. G. Dixit, *Jpn. J. Appl. Phys.*, 1992, **31**, 35.
23 J. H. Choy, Y. S. Han, J. T. Kim and Y. H. Kim, *J. Mater. Chem.*, 1995, **5**, 57.
24 J. H. Choy, Y. S. Han, Y. H. Kim and K. S. Suh, *Jpn. J. Appl. Phys.*, 1993, **32**, 1154.
25 J. H. Choy, Y. S. Han, S. W. Song and S. H. Chang, *J. Mater. Chem.*, 1994, **4**, 1271.
26 J. H. Choy, Y. S. Han and Y. H. Kim, *Mater. Lett.*, 1993, **16**, 226.
27 J. H. Choy, Y. S. Han and S. W. Song, *Mater. Lett.*, 1994, **19**, 257.
28 J. H. Choy, Y. S. Han and J. T. Kim, *J. Mater. Chem.*, 1995, **5**, 65.
29 F. M. M. Morel, *Principles of Aquatic Chemistry*, John Wiley & Sons, New York, 1983.
30 S. Morgan, *Aquatic Chemistry*, John Wiley & Sons, New York, 1983.
31 G. M. H. Van De Velde and J. Venselaar, *J. Inorg. Nucl. Chem.*, 1977, **39**, 1363.
32 L. N. Klatt, *Anal. Chem.*, 1970, **42**, 1837.
33 T. Meites and L. Meites, *J. Am. Chem. Soc.*, 1951, **73**, 1161.
34 D. R. Turner, M. Whitfield and A. G. Dickson, *Geochim. Cosmochim. Acta*, 1991, **45**, 855.
35 C. F. Baes and R. E. Mesmer, *The Hydrolysis of Cations*, Wiley & Sons, New York, 2nd edn., 1976.
36 L. M. Zaitsev and G. S. Bochkarev, *Zh. Neorg. Khim.*, 1964, **9**, 2122.
37 A. K. Babko and L. I. Dubovenko, *Izvest. Vyssh. Uchebn. Zaved, Khim. Khim. Technol.*, 1960, **3**, 226.
38 H. Bilinski, M. Branica and L. G. Sillen, *Acta Chem. Scand.*, 1966, **20**, 853.
39 H. Bilinski, B. Pokric and Z. Pucar, *J. Inorg. Nucl. Chem.*, 1971, **33**, 3409.
40 S. Bhattacharjee, M. K. Parica and H. S. Muiti, *Ceram. Int.*, 1992, **18**, 295.
41 A. K. Babko and L. I. Duvobenko, *Zh. Neorg. Khim.*, 1959, **4**, 372.
42 H. Jaffe, *IRE Proc.*, 1961, 1161.

Paper 7/00391I; *Received* 16*th January*, 1997